Dimeric valence-bond structures in correlated systems

A. A. Ovchinnikov and M. Ya. Ovchinnikova

Institute of Chemical Physics, Russian Academy of Sciences, 117977 Moscow, Russia

Correlated states with a regular dimeric structure of oriented valence bonds are studied for the 2D Hubbard model, which gives a single-band representation of the CuO_2 plane in a high-T_c superconductor. The correlated state is constructed by subjecting an uncorrelated state to local unitary transformations and then minimizing the energy with respect to a transformation parameter. An analog of the order parameter for describing valence-bond structures by mean-field methods with arbitrary doping is thereby introduced for the first time. A phase diagram is obtained for two types of states aligned along the bonds, viz., a spiral spin state and a valence-bond structure. The region of compatibility with antiferromagnetic ordering of the spins is found. The characteristic features of the excitation spectrum and the form of the Fermi boundary in the correlated system are discussed, in particular, in light of the observed photoelectron spectra of high-T_c superconductor single crystals. © *1996 American Institute of Physics.* [S1063-7761(96)02607-8]

1. INTRODUCTION

Exhaustive reviews describing the current state of the theory of electron correlations in high-T_c superconductors were given in Refs. 1 and 2. The creation of a microscopic theory of high-T_c superconductors requires knowledge of the electronic structure near the Fermi surface. Prospects in this area are tied to recent measurements of high-resolution angle-resolved photoelectron spectra (ARPES) of single crystals of lanthanum, yttrium, and bismuth ceramics (see Refs. 3–6 and the literature cited in Refs. 1 and 3). The main features of these photoelectron spectra include the small width of the bands in comparison to the calculated values, the presence of flat portions of the bands near the points $\bar{M} = (0, \pi)$ and $(\pi, 0)$, the characteristic nesting corresponding to quasimomentum near $Q = (\pi, \pi)$ for $Bi_2Sr_2CaCu_2O_{8+\delta}$, and the gap below the flat band in $Nd_{2-x}Ce_xCuO_4$. It would be natural to ask to what extent these features are due to electron correlations, and whether there are real electronic structures of a strongly correlated 2D system that could be responsible for the observed spectra.

Among the hypothetical structures of the effective single-band Hubbard problem,[7-10] which models the CuO_2 plane in a high-T_c superconductor, spin-density waves,[11] spiral spin states of various symmetry,[12,13] domain walls,[13,14] and various mixed states[15] have been investigated. It would be interesting to extend these investigations to states with regular dimeric valence-bond structures and to discuss the possible experimental manifestations of such states. Valence-bond states were first introduced by Anderson.[16] An analog of the order parameter for valence-bond states, which would permit the application of the mean-field methods that are so convenient for studying doped systems, however, was not proposed. The wave function of an essentially correlated state with dimeric valence-bond structures was constructed for the undoped 2D Hubbard model ($n = 1$) in Ukrainskiĭ's work.[17,18]

Our goal is to extend the description of such structures to doped systems, to investigate their stability, their compatibility with antiferromagnetic order and the form of the Fermi surface, and the possible manifestations of such structures in photoelectron spectra. A state with a regular dimeric valence-bond structure is constructed using local unitary transformations of the Hamiltonian with subsequent treatment of the effective problem by the mean-field method. The possibility of an exact calculation of the energy and minimization with respect to a transformation parameter (which is similar to minimization with respect to the incommensurate quasimomentum of spiral states) is important. In the present work we study dimeric structures of only one symmetry with valence bonds of one orientation.

Due to the small differences between the energies of the different hypothetical electronic structures of the correlated states, the realization of only one of them in a high-T_c superconductor is doubtful. However, the distinct observation of the Fermi surface and the bands, i.e., characteristics which are very sensitive to the structure of a correlated state, in ARPES and other experiments employing single crystals calls for serious consideration of the feasability of a particular structure and a discussion of its observable consequence.

2. USE OF LOCAL UNITARY TRANSFORMATIONS TO CONSTRUCT DIMERIC VALENCE-BOND STRUCTURES

We illustrate the idea of constructing such structures on a complex consisting of two centers with the orbits a and b and the parameters U and t for one-center repulsion and hopping. We consider a state with two holes in the complex. When $U/t > 1$, localization of each hole on a center and thus a decrease in the weight of the two-hole site configurations in comparison to their weight in the Hartree–Fock state can be achieved in two ways. One, which is widely known, is to transform to an antiferromagnetic function of the generalized Hartree–Fock method with different orbits for different spin projections. The other is to rotate in the basis of singlet states of the complex:
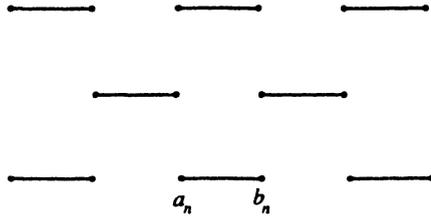
FIG. 1. Valence-bond structure calculated in the present work.

$$\Psi_{HF}=|f_\uparrow^+ f_\downarrow^+\rangle \rightarrow \Psi=|\cos\alpha f_\uparrow^+ f_\downarrow^+ - \sin\alpha \widetilde{f}_\uparrow^+ \widetilde{f}_\downarrow^+\rangle. \tag{1}$$

Here

$$f_\sigma=(a_\sigma+b_\sigma)/\sqrt{2} \quad \text{and} \quad \widetilde{f}_\sigma=(a_\sigma-b_\sigma)/\sqrt{2} \tag{2}$$

correspond to bonding and antibonding orbits (for $t<0$).

We now consider the 2D Hubbard model on a square lattice

$$H=\sum_n U n_{n\uparrow} n_{n\downarrow} + t\sum_\sigma \sum_{\langle nm\rangle} c_{n\sigma}^+ c_{m\sigma}. \tag{3}$$

The "internal structure" of the site states and the parameters of the effective single-band model are presently well understood and can be accurately evaluated using several cluster models of the CuO_2 plane in high-T_c superconductors.[9,10,19,20] For us it is significant that the new single-band problem is still strongly correlated ($U/t>1$). Our goal is to take these correlations into account.

A very pretty function of a correlated state, in which the role of the orbits f and $\widetilde{f}$ of the nonoverlapping complexes is played by Wannier orbits centered midway between the atoms comprising the dimer, was constructed for the undoped case ($n=1$) in Refs. 17 and 18. The structure of the dimers under consideration is shown in Fig. 1. However, the function from Refs. 17 and 18 was not generalized to doped systems. In addition, because of the small number of variational parameters, it corresponded to a higher energy than did the antiferromagnetic function of the standard generalized Hartree–Fock method.

To construct a general ($n \neq 1$) correlated state with the dimeric valence-bond structure shown in Fig. 1, we use the variational method of local unitary transformations (previously[19,20] applied to the single-band model of the CuO_2 plane).

The wave function Ψ of the correlated state can be represented as the result of a unitary transformation of the uncorrelated wave function of the Hartree–Fock approximation or the generalized Hartree–Fock method:

$$\Psi=W\Phi, \quad W=\prod_n W_n(a_n b_n),$$

$$n=(n_x n_y), \quad n_x+n_y=2k, \quad a_{n\sigma}=c_{n\sigma}, \tag{4}$$

$$b_{n\sigma}=c_{m\sigma}, \quad m=n+e_x.$$

Here each of the local unitary operators W_n is assigned to the nth cluster $\{a_n,b_n\}$, which includes two nearest-neighbor

lattice sites (Fig. 1). The operators W_n preserve the number of particles and the spin projection onto the cluster, and commute with one another.

Then the problem (3), with Hamiltonian H in the basis of correlated states Ψ, is equivalent to the problem with the transformed Hamiltonian

$$\widetilde{H}=W^+ HW \tag{5}$$

in the basis of uncorrelated one-determinant functions. Unlike Gutzwiller's nonunitary local transformation,[21] for (5) we can find an explicit expression of $\widetilde{H}$ in terms of the Fermi operators of the system and perform an accurate, albeit cumbersome, calculation of the energy for the Hartree–Fock functions Φ.

An arbitrary unitary operator W_n can be expressed in terms of the even Hubbard operators of the two-site complex $\{a_n,b_n\}$. To choose the form of W_n we take into account the following. Consideration of the correlations in the Hubbard model is most necessary for a mean number of particles per site $n\simeq 1$ or a mean number of particles in a cluster $n^a+n^b\simeq 2$, since in the limit $n\to 0$ or $n\to 2$ the Hartree–Fock approximation is exact. Therefore, we choose W_n as the unitary rotation operator of the basis of only the singlet two-hole components of the cluster:

$$|2i\rangle_n=\{|a_{n,\uparrow}^+ a_{n\downarrow}^+\rangle, |b_{n,\uparrow}^+ b_{n\downarrow}^+\rangle, (1/\sqrt{2})|\sum_\sigma(-\zeta_\sigma)a_{n\sigma}^+ b_{n,-\sigma}^+\rangle\}_i,$$

$$i=1,2,3, \quad \zeta_\sigma=-\sigma/|\sigma|=\mp 1. \tag{6}$$

Then W_n can be written in the form

$$W_n=I+\sum (S_{ij}-\delta_{ij})X_{2i,2j}^{(n)}. \tag{7}$$

Here the $X_{2i,2j}^{(n)}$ are the Hubbard operators in the basis of the states (6).

Thus, W_n is completely defined by the (as yet arbitrary) unitary matrix S_{ij}. The choice of the latter is suggested by the transformation (1), which is effected by the operator

$$W_n= \exp\{\alpha[\widetilde{f}_\uparrow^+ \widetilde{f}_\downarrow^+ f_\downarrow f_\uparrow - H.c.]\},$$

$$f_\sigma(\widetilde{f}_\sigma)=(a_\sigma\pm b_\sigma)/\sqrt{2}. \tag{8}$$

It is not difficult to see that in the representation (7) this operator corresponds to the unitary matrix

$$S_{ij}(\alpha)=\begin{pmatrix} c_+ & c_- & -\xi \\ c_- & c_+ & -\xi \\ \xi & \xi & c_\alpha \end{pmatrix}_{ij}, \tag{9}$$

$$c_\alpha=\cos\alpha, \quad c_\pm=(\cos\alpha\pm 1)/2, \quad \xi=\sin\alpha/\sqrt{2}.$$

Expressions for several Hubbard operators in terms of $a_{n\sigma}$ and $b_{n\sigma}$ are given in the Appendix.

We find an explicit expression for the Hamiltonian (5) of the new effective problem:

$$\widetilde{H}=\sum_n \widetilde{h}_n+\sum_l \widetilde{T}_l, \quad l=\{e_x\pm e_y, 2e_x\}, \tag{10}$$

$$\widetilde{h}_n=W_n^+ h_n W_n,$$

A. A. Ovchinnikov and M. Ya. Ovchinnikova   185

$$\mathbf{h}_n = U(\mathbf{n}_{n\uparrow}^a \mathbf{n}_{n\downarrow}^a + \mathbf{n}_{n\uparrow}^b \mathbf{n}_{n\downarrow}^b) + t\sum_n (\mathbf{a}_{n\sigma}^+ \mathbf{b}_{n\sigma} + \text{H.c.}), \qquad (11)$$

$$\widetilde{\mathbf{T}}_l = t\sum_{n,\sigma} (\widetilde{\mathbf{b}}_{n\sigma}^+ \widetilde{\mathbf{a}}_{n+l,\sigma} + \text{H.c.}). \qquad (12)$$

The summation is carried out only over the even $\mathbf{n}$ ($n_x + n_y = 2m$) labeling the clusters.

Each of the transformed operators $\widetilde{\mathbf{h}}_n$, $\widetilde{\mathbf{a}}_n$, or $\widetilde{\mathbf{b}}_n$ assigned to the nth cluster can be expressed explicitly in terms of the Hubbard operators of a two-site cluster in the basis of singlet two-hole components (6) and the one- and three-hole cluster functions

$$|1\lambda\sigma\rangle = \{|\mathbf{a}_{n\sigma}^+\rangle, |\mathbf{b}_{n\sigma}^+\rangle\}_\lambda, \quad \lambda = a, b, \qquad (13)$$

$$|3\lambda\sigma\rangle = \{|\mathbf{b}_{n\sigma}^+ \mathbf{a}_{n\uparrow}^+ \mathbf{a}_{n\downarrow}^+\rangle, |\mathbf{a}_{n\sigma}^+ \mathbf{b}_{n\uparrow}^+ \mathbf{b}_{n\downarrow}^+\rangle\}_\lambda, \quad \lambda = a, b. \qquad (14)$$

Specifically

$$\widetilde{\mathbf{h}}_n = \mathbf{h}_n + \sum (S_{ij}S_{i'j'} - \delta_{ij}\delta_{i'j'})h_{2i,2i}^0 \mathbf{X}_{2j,2j'}^{(n)}, \qquad (15)$$

$$\widetilde{\mathbf{a}}_{n\sigma} = \mathbf{a}_{n\sigma} + \sum (S_{ij} - \delta_{ij})x_{1\lambda-\sigma,2i}^a \mathbf{X}_{1\lambda-\sigma,2j}^{(n)}$$

$$+ (S_{ij} - \delta_{ij})x_{2i,3\lambda\sigma}^a \mathbf{X}_{2j,3\lambda\sigma}^{(n)}. \qquad (16)$$

The expression for $\widetilde{\mathbf{b}}_{n\sigma}$ is analogous to (16) with the replacements $\mathbf{a} \to \mathbf{b}$ and $x^a \to x^b$.

The quantities $h_{2i,2j}^0$, $x_{2j,3\lambda\sigma}^{a(b)}$, and $x_{1\lambda-\sigma,2j}^{a(b)}$ presented in the Appendix are the coefficients in the expansion of the original operators $\mathbf{h}_n$, $\mathbf{a}_{n\sigma}$, and $\mathbf{b}_{n\sigma}$ in the Hubbard operators in the basis of the cluster functions (6), (13), and (14), and are equal to the corresponding matrix elements of these operators.

Substituting the expressions (A1), (A2), etc. for the Hubbard operators into (15) and (16) and then into (10)–(12), we obtain the final explicit expression for the complete transformed Hamiltonian in terms of the Fermi operators of the system. In particular, h_n is expressed in terms of the even operators (A1), and the intercluster contributions to (10) can be rewritten in the form

$$\mathbf{T}_l = \sum_n g_{ij}^b g_{i'j'}^a \{\mathbf{q}_{ni}^+(\sigma)\mathbf{q}_{mi'}(\sigma)\mathbf{Q}_{nj}^+(-\sigma)\mathbf{Q}_{mj'}(-\sigma) + \text{H.c.}\},$$

$$\mathbf{m} = \mathbf{n} + 1. \qquad (17)$$

Here the operators $\mathbf{q}$ and $\mathbf{Q}$ referring to cluster $n(m)$ are

$$\mathbf{q}_{ni}(\sigma) = \{\mathbf{a}_{n\sigma}, \mathbf{b}_{n\sigma}, \mathbf{a}_{n\sigma}\mathbf{n}_{n\sigma}, \mathbf{b}_{n\sigma}\mathbf{n}_{n\sigma}\}_i, \quad i = 1, \dots, 4,$$

$$\mathbf{Q}_{nj}(s) = \{1, \mathbf{n}_{ns}^a, \mathbf{n}_{ns}^b, \mathbf{n}_{ns}^a\mathbf{n}_{ns}^b, \rho_{ns}^{ab}, \rho_{ns}^{ba}\}_j, \quad j - 1, \dots, 6, \qquad (18)$$

$$\rho_{ns}^{ab} = (\rho_{ns}^{ba})^+ = \mathbf{a}_{ns}^+ \mathbf{b}_{ns}.$$

The coefficients $g^{a(b)}$ can be recovered from (16) and (A2)–(A6).

As a result, we can accurately calculate the mean energy

$$\langle H \rangle = \langle \Psi H \Psi \rangle = \langle \Phi \widetilde{H} \Phi \rangle$$

for the correlated state Ψ constructed from the arbitrary uncorrelated (one-determinant) function Φ. More specifically,

$\langle H \rangle$ can be expressed explicitly in terms of one-electron averages $\langle c_{n\sigma}^+ c_{m\sigma}\rangle_\Phi$ over Φ. The minimization of $\langle H \rangle$ with respect to Φ for a given transformation parameter α is accomplished by self-consistently solving the linearized problem ($\widetilde{H}_L$). Subsequent minimization with respect to α determines the degree of stability of the structures involved in the transformation with alternation of the singlet pairing force in the bonds.

3. LINEARIZATION SCHEME AND PROPERTIES OF SELF-CONSISTENT SOLUTIONS

We describe the solution scheme for the valence-bond structure shown in Fig. 1.

The state with antiferromagnetic ordering of the spins in the sublattices $\{a_n\}$ and $\{b_n\}$ corresponds to the one-determinant function Φ of the generalized Hartree-Fock approximation. At the same time, when α is nonzero, the transformation $\mathbf{W}(\alpha)$ introduces some inequivalence into the intracluster and intercluster bonds ($a_n b_n$ and $b_n a_{n+l}$), $\mathbf{l} = \mathbf{e}_x \pm \mathbf{e}_y$, $2\mathbf{e}_x$ in the new problem $\widetilde{H}$. As a result, with consideration of the symmetry in the most general case, the mean energy $\bar{H} = \langle H \rangle$ depends on 11 real quantities:

$$y_\nu = \{\rho_0, \delta_0, \gamma_0, \rho_1, \delta_1, \gamma_1, \beta_1, \rho_2, \delta_2, \gamma_2, \beta_2\}_\nu,$$

$$\nu = 1, \dots, 11. \qquad (19)$$

These are combinations of one-electron averages over the state Φ:

$$\rho_i + \zeta_\sigma \delta_i = \langle \mathbf{a}_{n\sigma}^+ \mathbf{a}_{m\sigma}\rangle_\Phi = \langle \mathbf{b}_{n,-\sigma}^+ \mathbf{b}_{m,-\sigma}\rangle_\Phi,$$

$$\gamma_i + \beta_i = \langle \mathbf{a}_{n\sigma}^+ \mathbf{b}_{m\sigma}\rangle_\Phi = \langle \mathbf{a}_{n,-\sigma}^+ \mathbf{b}_{m,-\sigma}\rangle_\Phi, \qquad (20)$$

$$\gamma_i - \beta_i = \langle \mathbf{b}_{n\sigma}^+ \mathbf{a}_{m\sigma}\rangle_\Phi = \langle \mathbf{b}_{n,-\sigma}^+ \mathbf{a}_{m,-\sigma}\rangle_\Phi.$$

Here $\zeta_\sigma = -\sigma/|\sigma| = \mp 1$ and $\mathbf{m} = \mathbf{n} + \mathbf{l}_i$, where $\mathbf{l}_i = (0,0)$, $(1,1)$, or $(2,0)$ for $i = 0$, 1, and 2. The parameter $\beta_0 \equiv 0$ was not included in (19).

From the explicit dependence $\bar{H}(y_\nu)$ we find the linearized Hamiltonian

$$\bar{H}_L = \sum_{k,\sigma} \widehat{\mathbf{h}}_{k\sigma} + \bar{H} - \sum_\nu \frac{\partial \bar{H}}{\partial y_\nu} y_\nu, \qquad (21)$$

$$\widehat{\mathbf{h}}_{k\sigma} = \left\{ A_k \delta_{ij} + \begin{pmatrix} \zeta_\sigma \Delta_k & V_k' + iV_k'' \\ V_k' - iV_k'' & -\zeta_\sigma \Delta_k \end{pmatrix}_{ij} \right\}$$

$$\times \begin{pmatrix} \mathbf{a}_{k\sigma}^+ \\ \mathbf{b}_{k\sigma}^+ \end{pmatrix}_i \begin{pmatrix} \mathbf{a}_{k\sigma} \\ \mathbf{b}_{k\sigma} \end{pmatrix}_j, \qquad (22)$$

$$\{A_k, \Delta_k, V_k'\}_\mu$$

$$= \frac{1}{4}\sum_{\nu=0}^2 \left\{ \frac{\partial \bar{H}}{\partial \rho_\nu}, \frac{\partial \bar{H}}{\partial \delta_\nu}, \frac{\partial \bar{H}}{\partial \gamma_\nu} \right\}_\mu$$

$$\times \cos k_x l_x \cos k_y l_y, \qquad (23)$$

$$V_k'' = \frac{1}{4}\sum_{\nu=1}^2 \frac{\partial \bar{H}}{\partial \beta_\nu} \sin k_x l_x \cos k_y l_y. \qquad (24)$$

A. A. Ovchinnikov and M. Ya. Ovchinnikova   186

In the expressions under the summation sign $l=l(\nu)=(l_x,l_y)=(0,0)$, (1,1), or (2,0) for $\nu=0$, 1, and 2, and the quasimomentum runs through values in half of the Brillouin zone of the original square lattice.

The solution of the linearized problem for a fixed number of particles makes it possible to calculate the averages (20) and thereby complete the self-consistent calculation procedure. Here the eigenfunctions and eigenenergies h_k equal

$$\chi^+_{\lambda k\sigma}=\frac{1}{\sqrt{2}}\begin{pmatrix} c_k+\zeta_\sigma s_k & c_k-\zeta_\sigma s_k \\ c_k-\zeta_\sigma s_k & -c_k-\zeta_\sigma s_k \end{pmatrix}_{\lambda i}\begin{pmatrix} e^{i\vartheta_k}\mathbf{a}^+_{k\sigma} \\ e^{-i\vartheta_k}\mathbf{b}^+_{k\sigma} \end{pmatrix}_i,$$
(25)

$$E_k^{1(2)}=A_k+[\Delta_k^2+V_0^2]^{1/2}, \quad V_0^2=(V_k')^2+(V_k'')^2,$$
(26)

$$c_k=\cos\phi_k, \quad s_k=\sin\phi_k, \quad \tan(2\phi_k)=-\Delta_k/V_0,$$

$$\tan(2\vartheta_k)=V_k''/V_k'.$$

These correspond to the upper and lower Hubbard bands. The two subbands are preserved even in the absence of antiferromagnetic order because of the alternation of the singlet pairing force. In the absence of an interaction ($U=0$), the solution with $\alpha=0$, $\phi_k=0$, and $\vartheta_k=-k_x/2$ naturally coincides with the accurate Hartree–Fock solution for this case.

For an undoped system ($n=1$), the complete solution $\Psi=W\Phi$ is an analog of the solution constructed in Refs. 17 and 18. Apart from the form, there are three more differences.

1) Our solution is also valid for a doped system and not just for $n=1$, as in Refs. 17 and 18.

2) The one-electron spectrum of the linearized effective problem $\tilde{H}_L$ reflects the excitation spectrum of the correlated system for states with a regular dimeric valence-bond structure (see below).

3) The solutions for $n=1$ differ with respect to the number of variational parameters.

In our treatment, the variational parameters are the ϕ_k and ϑ_k for each k, and the self-consistent calculation procedure is simply minimization with respect to them and then with respect to α. At the same time, the solution in Refs. 17 and 18 is characterized by only three variational parameters: ϕ_0 (instead of the ϕ_k), the parameter λ in the rigorous dependence $\vartheta_k=\lambda k_x/2$, and an analog of α, i.e., the mixing parameter of the components of the singlet functions in the hole localization mechanism (1). Therefore, the energy of the undoped Hubbard model is lower in our method than in Refs. 17 and 18.

4. EXCITED STATES OF THE CORRELATED SYSTEM

The question of excited states has a direct bearing on the interpretation of photoelectron spectra.

In the new effective problem of $\tilde{H}(\alpha)$ treated in the independent-particle approximation (in the Hartree–Fock method or the generalized Hartree–Fock method), hole- and electron-type Fermi excitations with quasimomentum k and spin projection σ for $n\geq 1$ are given by the expressions

$$\Phi^h_{k\sigma}=\chi^+_{2k\sigma}\Phi_0, \quad \Phi^e_{\lambda k\sigma}=\chi_{\lambda k\sigma}\Phi_0, \quad \lambda=1,2,$$
(27)

where χ^+ (χ) creates a hole (electron) in the upper ($\lambda=2$) or lower ($\lambda=1$) Hubbard subbands for unoccupied (or occupied) orbits λk in the ground-state function. When $n\geq 1$, the latter equals

$$\Phi_0=\left|\prod_{k\in F}\prod_\sigma \chi^+_{2k\sigma}\prod_{k\sigma}\chi^+_{1k\sigma}0\right\rangle.$$
(28)

The band states of the hole representation are solutions of the linearized effective problem, and the product in (28) is taken over occupied orbits within the Fermi boundary.

Because of the unitary nature of the transformation, the correlated states

$$\Psi(k_i)=\mathbf{W}\Phi(k_i), \quad i=1,\dots,m$$
(29)

with different occupation numbers of the orbits $\chi_{\lambda k}$ in φ are correlated states with the excitation of m quasiparticles. They are normalized and orthogonal to one another and to the ground state $\Psi_0=W\Phi_0$. As in the simple Hartree–Fock approximation, the energies of the singly excited correlated states (29) are eigenvalues of the original Hamiltonian H to within second-order terms in $\mathbf{V}=\tilde{\mathbf{H}}(\alpha)-\tilde{\mathbf{H}}_L(\alpha)$, since

$$\mathbf{H}\Psi(\lambda k\sigma)=(E_0+E_{\lambda k})\Psi(\lambda k\sigma)+\mathbf{W}\mathbf{V}\Phi(\lambda k\sigma).$$

The first-order contribution in V to the excitation energy vanishes as a consequence of the self-consistent procedure for constructing the Hartree–Fock solution Φ_0.

We note that the quasiparticles in (29) are "dressed." The operators $\tilde{\chi}^+_{\lambda k\sigma}=\mathbf{W}^+\chi^+_{\lambda k\sigma}\mathbf{W}$, which play the role of the creation operators of an elementary excitation, also reflect many-particle effects in the correlated state. This can be seen from their explicit expression

$$\tilde{\chi}^+_{\lambda k\sigma}=(2/N)^{1/2}\sum_n e^{ikn}(S_{\lambda 1}g^a_{ij}+e^{ik_x}S_{\lambda 2}g^b_{ij})$$

$$\times q^+_{ni}(\sigma)Q^+_{nj}(-\sigma)$$

in terms of the many-fermion operators (18).

Thus, we now have a unique opportunity to describe both the ground and excited correlation states in the traditional language of the population of one-electron states. This is a significant advantage of local unitary transformations.

5. CALCULATIONS OF A DIMERIC STRUCTURE CONSISTING OF VALENCE BONDS HAVING THE SAME ORIENTATION

The numerical procedure for self-consistently solving the effective problem $\tilde{H}(\alpha)$ within the generalized Hartree–Fock method followed by minimization with respect to α was implemented for a structure consisting of x-oriented valence bonds (Fig. 1).

It was found that at any concentration $\delta=n-1$ of additional holes (n is the number of holes per site), the state with dimeric valence-bond structure (i.e., with $\alpha\neq 0$) is lower in energy than the standard antiferromagnetic solution obtained by the generalized Hartree–Fock method without alternation of bonds ($\alpha=0$). Antiferromagnetic order and the valence-bond structure coexist over a wide range of U/t and hole concentration. Figure 2 presents the dependence of the mean energy per bond (2 lattice sites) on U/t when

A. A. Ovchinnikov and M. Ya. Ovchinnikova   187
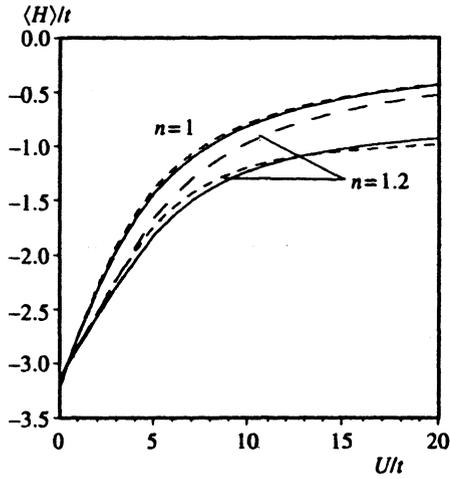
FIG. 2. Mean energy per bond $[H-2U(n-1)]$ calculated relative to its limiting value $2U(n-1)$ at $t=0$ as a function of U/t for hole concentrations $n=1$ and $n=1.2$. The solid curves correspond to states with dimeric valence-bond structures, and the short-dashed curves correspond to spiral states with $Q=(q,\pi)$. The long-dashed curve corresponds to an antiferromagnetic state with a dimeric valence-bond structure.

$n=1$ and $n=1.2$ for the correlated states with dimeric valence-bond structure (solid curves) and for spiral states with incommensurate quasimomentum $Q=(q,\pi)$. We calculated the latter using the equations in Ref. 13. In the undoped Hubbard model ($n=1$) the energies of the antiferromagnetic states with dimeric valence-bond structure (DS + AF) and without such a structure are very close. However, the difference increases with increasing n. The energy becomes less than the energy of the spiral state over a significant fraction of the parameter range.

Figure 3 presents the dependence of the spin density $\langle S_z \rangle$ in the a_n sublattice ($-\langle S_z \rangle$ in the b_n sublattice) and the transformation parameter α for the same hole concentrations $n=1$ and 1.2. When $U \to \infty$ and $n=1$, we have $\alpha \to -\pi/4$ at $t>0$. Inclusion of the hole-localization mechanism (1), which is an alternative to the antiferromagnetic
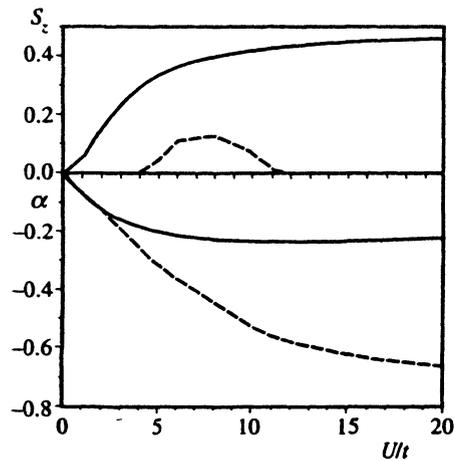
FIG. 3. Dependence of the spin density S_z on the sublattices and the transformation parameter α characterizing the formation of the valence-bond structure as a function of U/t for a hole concentration $n=1$ (solid curves) and $n=1.2$ (dashed curves).
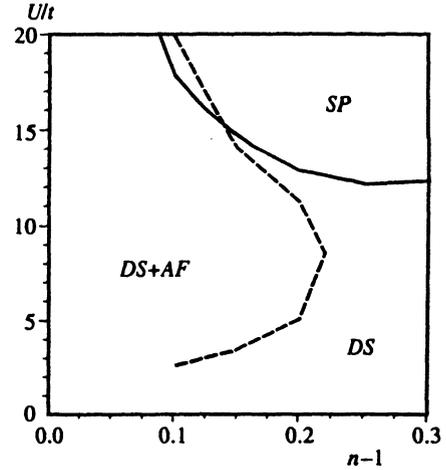
FIG. 4. Phase diagram for states with dimeric valence-bond structure and spiral states (SP) aligned along the x axis. The dashed curve demarcates the region where antiferromagnetic order exists along with dimeric structure.

mechanism, significantly lowers the magnetic moment $2\mu_B\langle S_z \rangle$ at the lattice sites in the DS+AF state.

Figure 4 presents the phase diagram in U/t and $\delta = n-1$ coordinates. The boundary of the region where dimeric valence-bond structure is more stable than the spiral state with $Q=(q,\pi)$ (SP) is indicated by the solid line. The dashed line marks the boundary for the disappearance of antiferromagnetic order in the complete solution of (4). We restrict ourselves here to a comparison of the solutions with the reference axis (x) along the bonds. Actually, according to Ref. 13, the spiral state with diagonal incommensurate quasimomentum $Q=(q,q)$ is lower than the state with $Q=(q,\pi)$. Therefore, it would be interesting to consider dimeric structures of the same symmetry containing both x- and y-oriented valence bonds. Calculations of the simplest of these structures with four sites in the unit cell is a matter for the future.

It was shown above that the spectrum of $E_{\lambda k}$ for the linearized Hamiltonian $\widetilde{H}_L$ reflects the spectrum of Fermi excitations of the correlated system against the background of the ground state of the particular electronic structure. Let us dwell on the properties of the spectrum of the dimeric valence-bond structure in Fig. 1. The picture of two Hubbard bands, a lower and an upper, is maintained for the doped case. The energies $(E_{\lambda k} - \mu)$ of the Hubbard bands for $n=1.2$ and $U/t=8$ along the $[\Gamma \overline{M}_x Y \Gamma]$ and $[\Gamma \overline{M}_y Y \Gamma]$ loops in the expanded (doubled) Brillouin zone $(-\pi \leqslant k_x, k_y \leqslant \pi)$ are presented in Fig. 5. The Γ, $\overline{M}_x$, $\overline{M}_y$, and Y points correspond, respectively, to $k=(0,0)$, $(\pi,0)$, $(0,\pi)$, and (π,π) (the notation of the points is the same as that of Ref. 5 and differs from that of Refs. 1 and 22). The distinguishing feature is the presence of flat portions of the bands at the points $\overline{M}_x$ and $\overline{M}_y$ that are asymmetric under the replacement $x \to y$. Within the basic Brillouin zone $(|k_x \pm k_y| \leqslant \pi)$ there are two very flat minima of the upper band (maxima of the lower band) on the x axis of the quasimomentum at the points $(\pm q_{min}, 0)$ near $\overline{M}_x = (\pi, 0)$, but there are no such features on the y axis. The depth and dis-

A. A. Ovchinnikov and M. Ya. Ovchinnikova   188
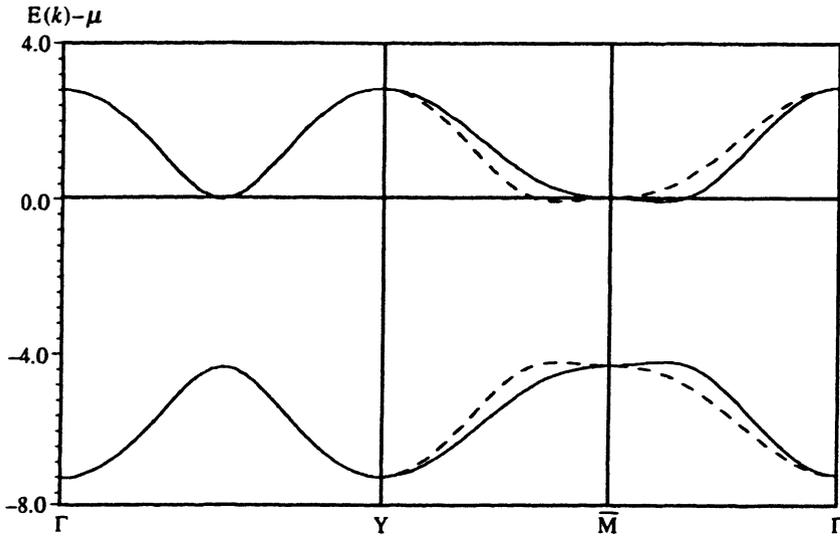
FIG. 5. Profile of the spectrum $E_{\lambda k} - \mu$ ($\lambda = 1$, 2) of eigenvalues of the linearized effective Hamiltonian $\tilde{H}_L$ along the $[\Gamma Y \bar{M}_x \Gamma]$ (solid curve) and $[\Gamma Y \bar{M}_y \Gamma]$ (dashed curve) loops for $n = 1.2$ and $U/t = 8$. The absolute values $|E_{\lambda k} - \mu|$ are the energies of the elementary Fermi excitations of the correlated system.

placement of the minimum from the point $\bar{M}_x$ increase with increasing U/t. When $\delta = n - 1$ or U/t is small, the asymmetry of the spectrum is small, and both $\bar{M}_x$ and $\bar{M}_y$ have energies lower than the Fermi level. In this case the Fermi surface has the form depicted in Fig. 6a in the space of the expanded Brillouin zone. However, above a certain value of U/t, the asymmetry causes only the region near $\bar{M}_x$ to be occupied in the upper band within the basic Brillouin zone ($|k_x \pm k_y| < \pi$). The energies $E_k = E_{\lambda - 2,k}$ for all k along the boundary $|k_x \pm k_y| = \pi$ of the basic Brillouin zone are essentially degenerate and are close to the chemical potential. For example, for $U/t = 8$ and $n = 1.2$, $(E_k - \mu)/t$ varies from -0.00206 to -0.00218 as k moves from the point $(\pi, 0)$ to the point $(\pi/2, \pi/2)$. Thus, part of the Fermi boundary essentially coincides with the lines $|k_x \pm k_y| = \pi$, displaying characteristic nesting with $Q = (\pi, \pi)$.

The features just described, i.e., the flat portions at the points $(\pi, 0)$ and $(0, \pi)$, the almost degenerate energies of the quasiparticles along the nesting line of the Hubbard lattice without an interaction ($|k_x \pm k_y| = \pi$), and the presence of a "large" Fermi surface instead of hole pockets in the vicinity of the points ($\pm \pi/2, \pm \pi/2$), were previously noted in the spectra of quasiparticles obtained from Monte Carlo

calculations of the Green's functions for the $t - J$ model[22] and in numerical simulations of the Hubbard model,[23-26] as well as in experimental photoelectron spectra.[3-6]

If it is assumed that a real single crystal of a ceramic contains a CuO_2 plane with structures consisting of x- and y-oriented valence bonds, an additional Fermi boundary analogous to the boundary depicted in Fig. 6b and symmetrically reflected about the $k_x = k_y$ line should be detected. Very similar boundaries with a characteristic nesting vector near $Q = (\pi, \pi)$, as well as boundary segments parallel to k_x and k_y, were observed in $Bi_2Sr_2CaCu_2O_{8+\delta}$ (Ref. 4). The flat portions of the spectra near $\bar{M}_x$ and $\bar{M}_y$ observed in the photoelectron spectra of all ceramics would be understandable under this hypothesis. We note that the observed profile of E_k along the $[\Gamma X \bar{M} \Gamma]$ loop in Refs. 3–6 was approximated by a one-band curve instead of two curves corresponding to upper and lower subbands. This might possibly have led to the conclusion that not only the nearest-neighbor lattice sites, but also the diagonally related next-nearest-neighbor sites interact. However, all the measurements pertain only to the $E_k^e - \mu < 0$ ($E_k^h - \mu < 0$) branches in the electron (or hole) representations, and are therefore not inconsistent with the two-band interpretation.
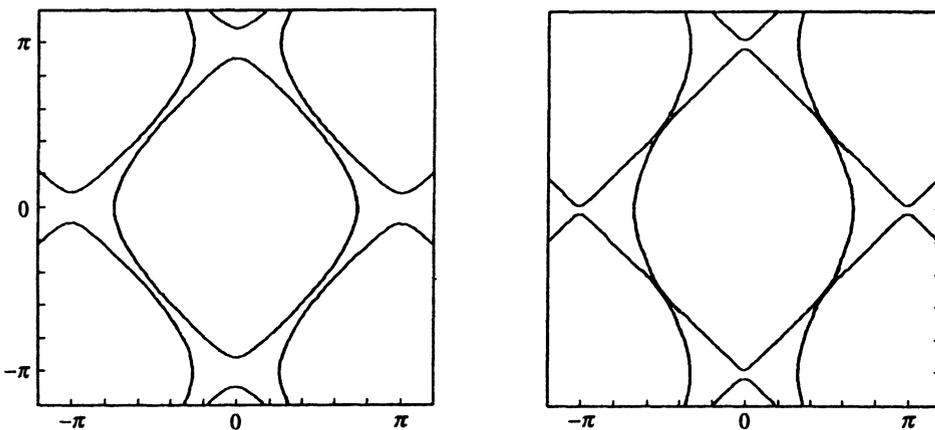
FIG. 6. Fermi surface in the expanded Brillouin zone for $n = 1.2$ when $U/t = 5$ (left-hand figure) and $U/t = 8$ (right-hand figure) in k_x, k_y coordinates.
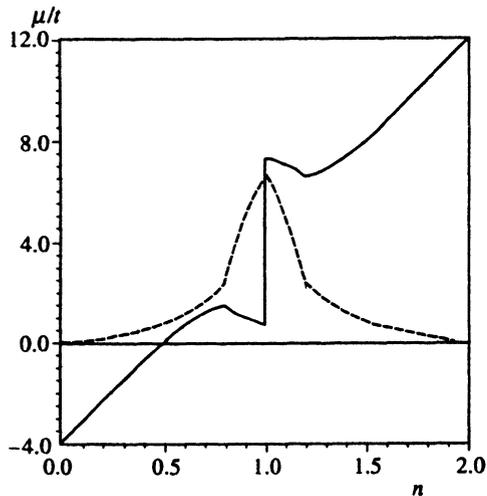
FIG. 7. Dependence of the chemical potential (solid curve) and the size of the gap between the upper and lower Fermi excitation bands (dashed curve) on the hole concentration for $U/t = 8$.

Figure 7 presents the dependence of the chemical potential and the size of the gap between the lower and upper bands of Fermi excitations on the hole concentration for $U/t = 8$. At the point where the antiferromagnetic order vanishes ($n \cong 0.8$ and 1.2) during electron and hole doping from the state of an undoped insulator ($n = 1$), the chemical potential is positive, and reaches a maximum (minimum) above or below the limits of $\mu(n)$ at $n = 1 \mp 0$. Together with the abruptly shrinking gap in the spectrum of quasiparticle excitations, this signals the emergence of a nonzero spectral density of states $N(\omega)$ within the insulating gap when $n = 1$. This conclusion is completely consistent with the calculations of the spectral functions for finite Hubbard systems,[25,26] where $N(\omega)$ is displaced within the gap upon the transition from electron to hole doping. The calculation and quantitative comparison of the spectral functions for correlated states with dimeric valence-bond structures and those obtained for finite systems by the Monte Carlo method or exact diagonalization represent a similar problem.

The large jump in μ between e- and h-doped systems observed both in the calculations of finite Hubbard systems[1,23-26] and in our own calculations is usually[1,25] thought to be inconsistent with the constancy of the chemical potential observed in photoelectron spectra. However, it was forgotten here that the doping of the CuO_2 plane in a sample that is neutral as a whole is accompanied by the appearance of alternating charge in the parallel layers, whose field should compensate the jump in μ of the isolated CuO_2 plane considered in the models.

The question of whether the entire body of data from photoelectron spectra can be attributed to the existence of dimeric x- and y-oriented structures calls for calculations of the spectral functions, particularly with consideration of the many-particle effects. Consideration of the latter becomes realistic for the class of correlated states treated here. The investigation must also be extended to structures of valences bonds of different symmetry aligned along $(e_x + e_y)$ and x- and y-oriented valence structures in a single CuO_2 plane.

6. CONCLUSIONS

The method proposed for constructing a correlated state by means of a unitary transformation of an uncorrelated state makes it possible to describe dimeric valence-bond structures for arbitrary doping. Mean-field methods have been successively used to describe such structures for the first time.

An explicit expression has been obtained for the Hamiltonian of the new effective problem, and an exact expression has been found for the mean energy. The many-particle creation operator of the elementary Fermi excitations of a correlated system with a given ground-state structure has been found.

The following results have been obtained for valence-bond structures with the same orientation.

(1) It has been shown that the correlated state with dimeric valence-bond structure is always more stable than the antiferromagnetic state of the generalized Hartree–Fock method, and that the energy difference increases with the concentration $\delta = n - 1$ of additional holes relative to the undoped system.

(2) When δ is small, the alternation of the singlet pairing force in the bonds in states with dimeric valence-bond structure is accompanied by antiferromagnetic ordering of the spins.

(3) The energy of the dimeric valence-bond structure investigated here lies below the energy of the spiral state of the same symmetry over a large range in δ and the strength of the interaction U/t.

(4) It has been shown for the dimeric valence-bond structure studied that the two Hubbard subbands in the spectrum of Fermi excitations of the correlated system are maintained upon doping. In accordance with the data from the photoelectron spectrum, the calculated spectrum is characterized by the presence of flat portions near the points $M = (\pi, 0)$ and $(0, \pi)$ and parallel portions of the Fermi boundary at large values of U/t (nesting with $Q = (\pi, \pi)$).

Investigations of valence-bond structures of different symmetry and direct calculations of the photoelectron spectra are needed to draw final conclusions regarding the existence of dimeric valence-bond structure in real single crystals, as well as their role in the shaping of the dynamic characteristics of the strongly correlated systems discovered by numerical modeling.[1]

APPENDIX A

Expressions for Hubbard operators

We present some of the Hubbard operators $X^{(n)}_{2i,2j}$, $X^{(n)}_{1\lambda-\sigma,2j}$, and $X^{(n)}_{2i,2\lambda\sigma}$ in a basis of the cluster functions (6), (13), and (14) (the superscript n is omitted below)

$$X_{2i,2j}$$

A. A. Ovchinnikov and M. Ya. Ovchinnikova   190

$$= \begin{pmatrix} \mathbf{P}_2^a\mathbf{P}_0^b & \mathbf{a}_\uparrow^+\mathbf{a}_\downarrow^+\mathbf{b}_\downarrow\mathbf{b}_\uparrow & \frac{1}{\sqrt{2}}\sum_\sigma \mathbf{a}_\sigma^+\mathbf{n}_{-\sigma}^a\mathbf{b}_\sigma(1-\mathbf{n}_{-\sigma}^b) \\ -\text{''}- & \mathbf{P}_0^a\mathbf{P}_2^b & \frac{1}{\sqrt{2}}\sum_\sigma \mathbf{b}_\sigma^+\mathbf{n}_{-\sigma}^b\mathbf{a}_\sigma(1-\mathbf{n}_{-\sigma}^a) \\ -\text{''}- & -\text{''}- & \frac{1}{\sqrt{2}}\sum_\sigma (\mathbf{P}_\sigma^a\mathbf{P}_{-\sigma}^b - \mathbf{a}_\sigma^+\mathbf{a}_{-\sigma}\mathbf{b}_\sigma^+\mathbf{b}_\sigma) \end{pmatrix}_{ij} . \quad \text{(A1)}$$

Here the missing elements are $\mathbf{X}_{2i,2j}=(\mathbf{X}_{2j,2i})^+$; $\mathbf{P}_0^a=(1-\mathbf{n}_\uparrow^a)(1-\mathbf{n}_\downarrow^a)$; $\mathbf{P}_2^a=\mathbf{n}_\uparrow^a\mathbf{n}_\downarrow^a$; $\mathbf{P}_\sigma^a=\mathbf{n}_\sigma^a(1-\mathbf{n}_{-\sigma}^a)$. The expressions for $\mathbf{P}_0^b$, $\mathbf{P}_2^b$, and $\mathbf{P}_\sigma^b$ are analogous.

The odd Hubbard operators in a basis of the functions (6) and the functions $|1\lambda\sigma\rangle$ and $|3\lambda\sigma\rangle$, where $\lambda=a$ and b, defined by Eqs. (13) and (14) can also be expressed in terms of Fermi operators. For example,

$$\mathbf{X}_{2i,3a\sigma}=\{\mathbf{b}_\sigma\mathbf{n}_\sigma^a\mathbf{n}_{-\sigma}^a(1-\mathbf{n}_{-\sigma}^b); -\mathbf{a}_\sigma\mathbf{n}^b\mathbf{b}_{-\sigma}^+\mathbf{a}_{-\sigma};$$
$$\qquad (\text{A2})$$
$$-\frac{1}{\sqrt{2}}[\mathbf{a}_\sigma\mathbf{n}_\sigma^b\mathbf{n}_{-\sigma}^a(1-\mathbf{n}_{-\sigma}^b)-\mathbf{b}_\sigma\mathbf{n}_\sigma^a\mathbf{b}_{-\sigma}^+\mathbf{n}_{-\sigma}]\}_i ,$$

$$i=1, 2, 3.$$

Expansion coefficients h_n, $a_{n\sigma}$, and $b_{n\sigma}$ for Hubbard operators

We present only the coefficients that appear in $\widetilde{\mathbf{H}}$ for the transformation (7), (9):

$$h_{2i,2j}^{(0)}=\langle 2i|\mathbf{h}|2j\rangle = \begin{pmatrix} U & 0 & t\sqrt{2} \\ 0 & U & t\sqrt{2} \\ t\sqrt{2} & t\sqrt{2} & 0 \end{pmatrix}_{ij} , \quad \text{(A3)}$$

$$x_{1\lambda\sigma,2j}(\mathbf{a}_{-\sigma})= \begin{pmatrix} \zeta_\sigma & 0 & 0 \\ 0 & 0 & \zeta_\sigma/\sqrt{2} \end{pmatrix}_{i\lambda j} , \quad \text{(A4)}$$

$$x_{1\lambda\sigma,2j}(\mathbf{b}_{-\sigma})= \begin{pmatrix} 0 & 0 & \zeta_\sigma/\sqrt{2} \\ 0 & \zeta_\sigma & 0 \end{pmatrix}_{i\lambda j} , \quad \text{(A5)}$$

$$x_{2j,3\lambda\sigma}(\mathbf{a}_\sigma)= \begin{pmatrix} 0 & 0 & -1/\sqrt{2} \\ 0 & 1 & 0 \end{pmatrix}_{i\lambda j} , \quad \text{(A6)}$$

$$x_{2j,3\lambda\sigma}(\mathbf{b}_\sigma)= \begin{pmatrix} 1 & 0 & 0 \\ 0 & 0 & -1/\sqrt{2} \end{pmatrix}_{i\lambda j} , \quad \text{(A7)}$$

Here $i_\lambda=1$, 2 for $\lambda=a$, b in the $|1\lambda\sigma\rangle$ and $|3\lambda\sigma\rangle$ states defined by Eqs. (13) and (14), and $\zeta_\sigma=-\sigma/|\sigma|=\mp1$.

[1] E. Dagotto, Rev. Mod. Phys. **66**, 763 (1994).
[2] G. Senator and N. H. March, Rev. Mod. Phys. **66**, 445 (1994).
[3] J. W. Allen, R. Classen, R. O. Anderson et al., in Proceedings of the NATO Workshop "The Physics and Mathematical Physics of the Hubbard Model," San Sebastian, 1993, D. K. Campbell, J. M. P. Carmelo, and F. Guinea (eds.) Plenum Press, New York (1994).
[4] K. Gofron, J. C. Campuzano, H. Ding et al., J. Phys. Chem. Solids **54**, 1193 (1993).
[5] D. S. Dessau, Z.-X. Shen, D. M. King et al., Phys. Rev. Lett. **71**, 2781 (1993).
[6] M. R. Norman, M. Randeria, H. Ding et al., Phys. Rev. B **52**, 615 (1995).
[7] F. C. Zhang and T. M. Rice, Phys. Rev. B **37**, 3759 (1988).
[8] V. J. Emery and G. Reiter, Phys. Rev. B **38**, 4547 (1988); **38**, 11 938 (1988); **41**, 7243 (1990).
[9] H.-B. Schuttler and A. J. Fedro, Phys. Rev. B **45**, 7588 (1992).
[10] J. H. Jefferson, H. Eskes, and L. F. Feiner, Phys. Rev. B **45**, 7959 (1992).
[11] J. R. Schrieffer, X.-G. Wen, and S.-C. Zhang, Phys. Rev. B **39**, 11 663 (1989).
[12] C. Jayaprakash, H. R. Krishnamurthy, and S. K. Sarker, Phys. Rev. B **40**, 2610 (1989).
[13] F. Hu, S. K. Sarker, and C. Jayaprakash, Phys. Rev. B **50**, 17 901 (1994).
[14] D. Poilblanc and E. D. Siggia, Phys. Rev. Lett. **62**, 1564 (1989).
[15] I. E. Dzyaloshinskii, Zh. Eksp. Teor. Fiz. **93**, 1487 (1987) [Sov. Phys. JETP **66**, 848 (1987)].
[16] P. W. Anderson, Science **235**, 1196 (1987).
[17] I. I. Ukrainskii and E. A. Ponezha, in Electron–Electron Correlation Effects in Low-Dimensional Conductors and Superconductors, I. I. Ukrainskii and A. A. Ovchinnikov (eds.) Springer, New York (1991), p. 92.
[18] I. I. Ukrainskii, Int. J. Quantum Chem. **52**, 413 (1994).
[19] A. A. Ovchinnikov and M. Ya. Ovchinnikova, Phys. Lett. A **187**, 83 (1994).
[20] A. A. Ovchinnikov and M. Ya. Ovchinnikova, J. Phys.: Condens. Matter **6** (47), 10 317 (1994).
[21] M. C. Gutzwiller, Phys. Rev. A **137**, 1726 (1965).
[22] E. Dagotto, A. Nazarenko, and M. Boninsegni, Phys. Rev. Lett. **73**, 728 (1994).
[23] A. Moreo, D. J. Scalapino, R. Sugar et al., Phys. Rev. B **41**, 2313 (1990).
[24] R. R. P. Singh and R. L. Glenister, Phys. Rev. B **46**, 14 313 (1992).
[25] E. Dagotto, A. Moreo, F. Ortolani et al., Phys. Rev. Lett. **67**, 1918 (1991).
[26] R. Preuss, W. Hanke, and W. von der Linder, Phys. Rev. Lett. **75**, 1344 (1995).